Mode-I interlaminar fracture toughness of flax, glass and hybrid flax-glass fibre woven composites: Failure mechanism evaluation using acoustic emission analysis

El Hadi Saidane, Daniel Scida, Marie-José Pac, Rezak Ayad

▶ **To cite this version:**

El Hadi Saidane, Daniel Scida, Marie-José Pac, Rezak Ayad. Mode-I interlaminar fracture toughness of flax, glass and hybrid flax-glass fibre woven composites: Failure mechanism evaluation using acoustic emission analysis. Polymer Testing, 2019, 75, pp.246-253. 10.1016/j.polymertesting.2019.02.022 . hal-02497644

HAL Id: hal-02497644
https://hal.univ-reims.fr/hal-02497644

Submitted on 22 Oct 2021

HAL is a multi-disciplinary open access archive for the deposit and dissemination of scientific research documents, whether they are published or not. The documents may come from teaching and research institutions in France or abroad, or from public or private research centers.

L'archive ouverte pluridisciplinaire **HAL**, est destinée au dépôt et à la diffusion de documents scientifiques de niveau recherche, publiés ou non, émanant des établissements d'enseignement et de recherche français ou étrangers, des laboratoires publics ou privés.

Distributed under a Creative Commons Attribution - NonCommercial 4.0 International License

Version of Record: https://www.sciencedirect.com/science/article/pii/S0142941819300765
Manuscript_350d5b8605486ed6db6f9c137c430e7e

Mode-I interlaminar fracture toughness of flax, glass and hybrid flax-glass fibre woven composites: failure mechanism evaluation using Acoustic Emission analysis

El Hadi Saidane[1]*, Daniel Scida[2], Marie-José Pac[1], Rezak Ayad[2]

[1]*Université de Haute Alsace, Laboratoire de Physique et Mécanique Textiles EA 4365, 68093 Mulhouse, France.*

[2]*Université de Reims Champagne Ardenne, LISM EA 4695, 51097 Reims, France.*

Abstract

The mode-I interlaminar fracture toughness of flax, glass and hybrid flax-glass fibre woven composites was studied by using a DCB test. The acoustic emission signals recorded during the tests and scanning electron microscope images were used to analyse the damage mechanism of each composite. The crack initiation for the flax-fibre laminate needs the highest energy (1079 versus 945 for hybrid flax-glass fibre and 923 J/m² for glass-fibre laminates). The morphology of the flax fibres, short and bonded together in bundles to manufacture the twill fabric, allows the creation of a larger amount of fibre bridging as the origin of this highest energy. Furthermore, hybridisation of glass fibres with flax fibres in an appropriate combination offers an interesting solution when the toughness of glass fibre composites needs to be increased. More interesting is the considerable advantage of the composite structure weight reduction due to the low flax fibre density.

Keywords: Flax fibre; hybrid woven composites; interlaminar fracture toughness; delamination; acoustic emission.

1. Introduction

For the past two decades, natural fibre-reinforced composites have been used in many industrial applications, especially in the automotive and construction sectors [1–7]. For example, the plant-based natural flax fibre shows great potential to be a suitable replacement for mineral-based basalt and synthetic glass fibres for crushable energy absorber application, as highlighted by Yan et al. [1,2]. Huang et al. [3] studied the possibility of the using flax fabric reinforced epoxy composite plates as external strengthening material for reinforced concrete beams. The results showed that the flax fabric reinforced polymer composite can be used to retrofit or strengthen deficiently-designed concrete structures as an environmentally-friendly external reinforcement material. In addition to their eco-friendly aspect and biodegradability [8], natural fibres present high specific properties [9], due to their low density [10,11], and an interesting damping behaviour [12]. Therefore numerous comprehensive

* Corresponding author. Tel.: +33 325 467 144

E-mail address: el-hadi.saidane@uha.fr

© 2019 published by Elsevier. This manuscript is made available under the CC BY NC user license
https://creativecommons.org/licenses/by-nc/4.0/

studies have been conducted on natural fibre composites [13–18]. However, the development of these green materials may be limited because of the low interfacial properties between hydrophilic fibres and the hydrophobic matrix, which leads to delamination between the composite plies, thus lowering the mechanical properties [19]. In addition, delamination may also occur due to the presence of residual stresses during the manufacturing process or in a changing environment because natural fibres are temperature and moisture sensitive. Accordingly, knowledge of the interlaminar properties of these materials is essential for the design of composite structures, in particular when they are composed of long continuous unidirectional fibres or woven fabrics. Within this context, some authors have analysed the interlaminar fracture properties of natural fibre composites [19–27]. For example, Bensadoun et al. [19] studied the influence of fibre architectures on the mode-I and mode-II interlaminar fracture toughness of flax fibre epoxy composites. They compared the fracture toughness of plain weave, twill weave and quasi-unidirectional architectures. The results showed that the flax composites exhibited a high interlaminar fracture toughness which was related to several energy absorbing mechanisms such as the crack branching and fibre bridging. By comparing the different fibre architectures, they showed that the yarn crimp and irregular surface of the layers could generate more energy consumption by forcing the crack to follow an irregular delamination path. In a similar study, Pinto et al. [20] demonstrated that jute fibre woven composites showed a greater initiation fracture toughness than unidirectional ones because of fibre bridging and increasing interaction in the intra-ply. Ravandi et al. [21] studied the effects of through-the-thickness stitching using natural fibres on the interlaminar fracture toughness and tensile properties of flax fibre/epoxy composites. They found that the fracture toughness of the laminates was more improved by flax yarn stitches compared to cotton thread stitches. Furthermore, the interlaminar fracture toughness of woven flax composites was significantly higher than that of glass fibre composites. The hybridisation effect on the interlaminar fracture properties of unidirectional flax/glass fibre reinforced hybrid composites was investigated by Zhang et al. [22] who found that the interlaminar shear strength and the interlaminar fracture toughness of hybrid flax/glass fibre composites were higher than those of glass fibre ones. This was explained by the rough surface of flax fibres, which led to more fibre bridging between flax fibres, flax yarn and glass fibres.

The work reported in this paper aims at evaluating the mode-I interlaminar fracture toughness of flax, glass and hybrid flax-glass fibre reinforced epoxy (FFRE, GFRE and HFRE) laminates. The choice of flax and glass fibres, which have comparable mechanical performances, aims at analysing the effect of their hybridisation on the interlaminar fracture properties of the HFRE composite and enables studying the delamination between flax and glass fibre layers. For this purpose, three twill weave fabric laminates (FFRE, GFRE and HFRE with a single stacking sequence) were manufactured by a compression moulding process. Then, the double cantilever beam (DCB) tests were conducted to evaluate the mode-I interlaminar fracture toughness properties. In addition, the DCB tests were monitored using the acoustic emission (AE) technique to identify the different damage mechanisms of these composites. This identification was made with an unsupervised method based on a statistical multivariable analysis (k-means algorithm) using Noesis software. Several previous studies used this method to assess the damage failures of natural fibre composites during different mechanical tests, in particular tensile tests [28–30], cyclic and fatigue tests [31]. However, to the best of our knowledge, this method was not yet employed to evaluate the damage mechanisms of natural fibre composites during DCB tests. In addition, scanning electron microscopy (SEM) was performed to observe and understand the different damage mechanisms previously identified by the AE results.

2. Experimental methods

2.1 Materials and manufacturing process

The fabric weave used for the laminated composites was a 2/2 twill weave. The flax fabric, based on untwisted yarns and provided by Depestele Group, had an areal weight of 350 g/m^2 and a fibre density of 1450 kg/m^3. The linear mass of the warp and weft yarns of the dry fabric was the same and equal to 300 Tex. The flax fibres were bonded together by a specific binder to form a flat roving and allow weaving. The glass fabric, supplied by Sicomin Company, had an areal weight of 300 g/m^2 and a fibre density of 2450 kg/m^3. The yarns distribution in the warp and weft directions was the same and equal to 50%. The matrix used for the laminated composites was an SR 1500 epoxy resin associated with SD 2503 hardener marketed by Sicomin Company. The mixing ratio of resin and hardener was

100:33 by weight.

FFRE, GFRE and HFRE composites with a single stacking sequence were manufactured by compression moulding. 450 mm × 300 mm laminate plates were prepared with a different number of layers as summarised in Table 1. These numbers were chosen to obtain approximately the same and minimum 4 mm thickness for all composites. The advantage of a single stacking sequence is to allow the study of the delamination between the flax and glass fibres layers in the middle plane of the HFRE composite. First, flax and glass fabrics were manually pre-impregnated with the resin system. Next, the impregnated layers were placed one over the other following the same orientation with resin layers. During the layup process, a 12 µm thick Teflon insert of thickness was inserted at the midplane of the laminate to form a precrack, i.e. an initiation site for delamination (Figure 1a). The whole assembly was carefully placed between two steel platens covered with Teflon paper. Laminates were then cured in a compression moulding machine (SATIM model) under 5-bar pressure at 35°C for 3 hours, following the supplier's recommendations. Finally, the laminate plates were cut and shaped in rectangular form (20 mm × 170 mm) according to ASTM D5528-13 standard [32] by using a diamond saw blade. The thickness and fibre volume fraction of different composites are also given in Table 1. The fibre volume fractions (V_f) of FFRE, GFRE and HFRE composites were experimentally determined by the same procedure detailed in Saidane et al [28].

2.2 Mode-I interlaminar fracture toughness testing

The mode-I interlaminar fracture toughness (G_{IC}) and the resistance curve (R-curve) were evaluated by the DCB tests in accordance with ASTM D5528-13 standard [32]. They were conducted on an Instron 3382 universal machine with a 5 kN capacity load cell. To produce steady crack growth, a cross-head speed of 5 mm/min was used. For each composite, five specimens were tested. The average value and the standard deviation were then reported. The specimen geometry and its nominal dimensions are depicted in Figure 1a. The initial delamination length, a_0, of all samples was 50 mm. A pair of piano hinge tabs was bonded to the end of each specimen, as shown in Figure 1a. Before bonding the hinges, surfaces of both sides were lightly scrubbed with sandpaper and wiped clean with

acetone. After surface preparation, the hinges were aligned parallel with the specimen and with each other, and bonded using a Penloc GTI glue (Adheko MMA-3295). Clamps were used to hold them in position for 48 h until the adhesive was fully cured. To make the detection of delamination onset easier, one side edge of each specimen was painted with white lacquer. The use of the AE technique enabled clear identification of the initiation of the crack when the cumulative number of AE hits significantly increases (Figure 2a).

The strain energy release rate G_{IC} is given by Modified Beam Theory (MBT), as follows [32]:

$$G_{IC} = \frac{3P\delta}{2b\left(a + |\Delta|\right)} \tag{1}$$

where P is the load, δ is the load point displacement, b is the specimen width and a is the delamination length. The crack length correction factor, Δ, was experimentally obtained by plotting the cube root of compliance, $C^{1/3}$, as a function of the delamination length (Figure 2b). The compliance C is the ratio of the load point displacement to the applied load, δ/P. To evaluate the factor, Δ, note that four samples with different initial delamination lengths, 30, 50, 60 and 70 mm, were used, and the compliance was determined for each sample.

2.3 Acoustic emission

To obtain information about damage evolution in the tested specimens, AE was continuously monitored during the delamination tests. AE measurements were conducted using two-channel data acquisition system, with a sampling rate of 5 MHz and 40 dB pre-amplification, produced by Mistras Group Company. This system was equipped with a PCI acquisition card connected to the microcomputer. AE signals were recorded by two resonant Micro-80 piezoelectric sensors with a frequency range of 100 kHz–1 MHz and a resonance peak of around 300 kHz. The sensors were placed on the upper surface of the test specimen with a spacing of 80 mm, as shown in Figure 1a. To provide a good acoustic coupling, a silicone grease was employed as a coupling agent between the sensors and the sample surface. Before the DCB tests, a pencil lead break procedure was used to optimise the distance between the two AE sensors. Then, the AE acquisition system was calibrated to record the signals located between the two sensors using the AE localisation method. The quality of

the measured AE data mainly depends on the chosen waveform system timing parameters. These parameters, namely, PDT (peak definition time), HDT (hit definition time) and HLT (hit lockout time), enable the selection of the event characteristics. For the composite material tests, the values of the timing parameters employed were: PDT = 30 μs, HDT = 200 μs and HLT = 300 μs. The main parameters measured on the AE event parameters are depicted in an example of AE waveform in Figure 1b.

3. Results and discussion

3.1 Mode-I interlaminar fracture properties

3.1.1 Load-displacement curves

The load-displacement curves of the mode-I DCB tests of FFRE, HFRE and GFRE composites are shown in Figure 3. For the three composites, the curves present an initial linear region corresponding to linear elastic behaviour followed by à non-linear region in which the initiation and propagation of the cracks occur. The latter depends on the type of composite. Delamination initiation was visually observed and detected by the first change in the slope of the AE cumulative hits number (Figure 2a). For the FFRE, after the initiation of cracks close to 39N, the load slowly increases with increasing displacement due to fibre bridging and, then, a steady crack appears. The GFRE composite exhibits the highest load, around 47 N. After the maximum load of 52 N, the load sharply drops with increasing displacement until the composite fails. The drop of this maximum corresponds to delamination onset at the precrack tip, i.e. the initiation and growth of the cracks in the laminate. In the case of HFRE composite, crack initiation is near 42N, an intermediate value between those of FFRE and GFRE. Moreover, a large amount of load drop occurs due to crack stop during the displacement increase.

Table 2 displays the values of initiation G_{Ic} obtained from Eq. 1 for FFRE, HFRE and GFRE composites. These values were determined by measuring the load and deflection at the point at which delamination occurred. The values of initiation G_{Ic} correspond to the initial delamination length (a_0 = 50 mm) and describe the resistance of the sample to crack formation. The FFRE composite has a

higher initial interlaminar fracture toughness than the GFRE and HFRE ones (Table 2). The interlaminar fracture toughness of the FFRE composite is approximately 1.2 times more than that of the GFRE composite (1079 J/m^2 for the FFRE laminate and 923 J/m^2 for the GFRE laminate). A similar tendency has already been observed by Zhang et al. [22] for unidirectional flax and glass fibre composites. In the same way, the FFRE laminate value was 17% greater than the GFRE laminate value, even though the fibre volume content of the FFRE composite (40%) was lower than that of the GFRE composite (50%). This difference in initiation G_{Ic} values can be explained by the morphology and the structure of flax and glass fibres, which are fully different. Indeed, during manufacturing of flax fabrics from short flax fibres, the short individual flax fibres are bonded together in bundles to make long natural yarns, so as to weave them into 2D fabrics. Therefore, some individual flax fibres stretch out from the yarns more easily, as shown in Figure 4a. This generated a large amount of fibre bridging, leading to a higher delamination resistance for the FFRE composite. In the case of the glass fabric, the fibres are long, continuous and present a regular structure and smooth surface. Accordingly, the GFRE composite shows fewer rough fracture surfaces and no fibre bridging (Figure 4b). The yarn crimp in the woven fabric can also explain this difference in G_{Ic} values. Indeed, Bensadoun et al. [19] showed that the yarn crimp and irregular surface of the layers forced the crack to follow an irregular path, hence, led to more consumption of energy. For our composites, the same results are observed since the waviness thickness of FFRE, which exhibits a larger G_{Ic}, is higher than that of GFRE (0.20 mm vs. 0.09 mm). In addition, the G_{Ic} value of the FFRE composite is higher than flax-epoxy woven composites with similar V_f (40%), studied by Bensadoun et al. [19]. Indeed, they found values of G_{Ic} equal to 607 J/m^2 and 754 J/m^2 for flax-epoxy twill composites with high and low twist yarns, respectively. This was mainly due to the twist angle of flax yarns because the G_{Ic} initiation value decreases with increasing twist angle. In our case, flax fabric was made up of untwisted yarns. For the HFRE composite, the value of G_{Ic} is approximately 945 J/m^2 rather close to the G_{Ic} value of the GFRE composite despite the difference of V_f between both composites (40% for HFRE vs. 50% for GFRE). Thus, if the fracture toughness of glass fibre composites needed to be increased; hybridisation of glass fibres with flax fibres in an appropriate combination would offer an interesting solution. This solution also reduces the composite structure weight as the density obtained for the HFRE composite is 1.4

times lower than that of the GFRE composite (Table 2). This is mainly due to the flax fibre density (1450 kg/m^3) which is significantly lower than that of the glass (2540 kg/m^3). These structural properties are interesting since HFRE composite presents a density gain of about 34% against the GFRE composite and at the same time, a gain in the specific fracture toughness (the ratio of G_{Ic} to the density of the material) of 37% (Table 2).

3.1.2 Resistance curves (R-curves)

In order to visually observe the crack propagation, the edge of each specimen was marked from the insert with vertical lines every 5 mm, as suggested by the ASTM standard [32]. The vertical lines correspond to crack lengths of 50, 55, 60, 65, 70, 75, 80, 90 and 100 mm and the corresponding load and cross-head displacement were recorded. Then, the values of G_{Ic} were calculated from Eq. 1 for each crack length. The obtained results are depicted as resistance curves (R-curves) in Figure 5, which displays the values of G_{Ic} as a function of the delamination lengths of each composite. One can notice that the G_{Ic} of the FFRE composite increases in a progressive way increasing the crack length. This was directly related to the increase in the amount of fibre bridging during the test. For the GFRE composite, a slight increase of G_{Ic} can be seen at the beginning of crack propagation followed by a steady state because no fibre bridging occurred. The initial increase at the beginning of the test can be explained by the presence of some resin-rich regions due to the manufacturing process, in particular at the crack tip, while the steady state is because no fibre bridging occurred during the test. Furthermore, the crack has a clear and easy path along the glass fibre layer with no deviation in the path (Figure 4b). Concerning the HFRE composite, a combination of both R-curves behaviours of the FFRE and GFRE laminates is observed. For crack lengths between 50 and 65 mm, the HFRE and FFRE composites follow the same tendency with increasing G_{Ic} values due to the increase of fibre bridging during the DCB test. So, in this region, the R-curve of the HFRE composite is governed by the flax fibres. When the crack length is over 65 mm, a difference is observed in FFRE and HFRE R-curves behaviour. While the G_{IC} values continue to increase for FFRE composite, they remain constant and higher for HFRE composite due to the presence of glass fibres. For crack lengths between 55 and 85 mm, the HFRE composite exhibits the largest propagation value of G_{Ic} compared to the other

composites because of the large amount of flax and glass fibre bridging (Figure 4c) and a deviation in the path of the crack which is not observed in FFRE specimens (Figure 4a). It could be due to the torn out glass fibres, which play a bridging role between the flax and glass fibre layers. The same phenomena were observed by Zhang et al. [22] for unidirectional flax/glass fibre reinforced hybrid composites.

3.2 Damage mechanisms analysis

3.2.1 Acoustic emission results

In order to assess the damage mechanisms in the studied specimens during DCB tests, the AE signals were recorded and analysed by considering a statistical multi-variable analysis using Noesis software. This method was employed to separate the acoustic signals into different classes presenting the same characteristics for each clustering signal. This classification was carried out by considering the main AE parameters, i.e. amplitude, duration, number of counts, energy and rise time, as reported in the literature [28,29,31]. To optimise the number of acoustic signals classes, a principal component analysis (PCA) on the 2D projection planes was considered, as shown in Figure 6. For each composite, the number of classes was varied (from 2–5) and the overlap rate between the various groups of AE signals was determined [28,30]. Next, the optimum number of classes was obtained by considering the minimum average value of the overlap rate between them. Three classes are obtained for the GFRE composite (Figure 6a) while four AE classes are optimum for the FFRE and HFRE composites, (Figure 6b).

In order to associate the obtained classes with their corresponding damage mechanisms, the characteristics of the recorded waveforms of each group of signals were analysed and compared with the literature results. Table 2 displays the AE characteristics of each signal clustering for the three studied composites. The signals of Class A are characterised by amplitude values ranged between 32–60 dB with duration and number of counts lower than 70 μs and 38, respectively. Moreover, the characteristics of these signals are substantially similar for the three composites and present very low energies (<100 aJ). Note that the epoxy matrix is the single component that is common to the three

composites. The same characteristics were obtained in literature results for unidirectional flax/Elium composites under tensile [29,31], cyclic and fatigue tests [31] indicating that class A can be associated with the matrix cracking mechanism. The signals of Classes B and C also appear for the three composites with identical characteristics. More precisely, the signals of Class B are identified at an amplitude between 39 and 68 dB, a duration of 48 to 216 μs and a number of counts between 18 and 107. These characteristics are assigned to the fibre-matrix debonding in accordance with the literature [29–31,33–36]. The class C presents signals characteristics (50–82 dB amplitude, 115–331 μs duration and 36–169 count range) slightly higher than those observed for the class B. According to Mitchell et al. [37], Class C can be attributed to the delamination mechanism. The last class, i.e. the Class D, detected at amplitudes up to 75 dB and high energy (>100000 aJ) for FFRE and HFRE composites is not observed for the GFRE composite for which no fibre bridging occurred during the delamination tests (Figure 4b). As a consequence, the last Class D, also observed in the literature results [28,29,31,35], can be associated with fibre failure mechanisms.

To illustrate the damage mechanisms during DCB tests, the evolution versus time and cross-head displacement of the cumulative number of hits of each class, combined with DCB load is shown in Figure 7 for the three composites. According to the shape of the cumulative hits number of the different classes, the curves are divided into three regions. The first region (Label I) corresponds to the failure-free domain, i.e. delamination onset has not yet occurred. In this first zone, only signals induced by matrix cracking appear with few events. The second and third regions (Labels II and III) are associated with the initiation and propagation of delamination, respectively. Region II is defined by crack initiation, corresponding to the slope change of the cumulative hits number of the matrix cracking and the maximal load. In this region and for all composites, the acoustic activity of the matrix cracking increased suddenly, accompanied by the acoustic events due to the beginning of the fibre-matrix debonding and delamination. For the FFRE and HFRE composites, the signals relative to the fibre failures also appear because of failures of some fibre bridging and the generation of a large amount of fibre bridging (Figures 4a and 4c). After delamination onset, the slope increase of the cumulative hits number for the four damage mechanisms of the FFRE composite was higher than that of the HFRE ones. This result is consistent with the higher value of G_{IC} of the FFRE composite. In

Region III, the acoustic activity of all damage mechanisms increases in a quasi-linear way until the final failure of the FFRE and HFRE composites. In contrast to Region II, the slope of the cumulative hits number of the four damage mechanisms is more important for the HFRE composite compared to the FFRE composite, probably due to the deviation of the crack path of the HFRE composite, which led to several flax fibres being torn out from the fractured surface of the flax layer. This could generate a large amount of fibre bridging at the propagation state leading to important distribution of the AE energy as well as an increase of the interlaminar fracture toughness of the HFRE composite. In the case of the GFRE composite in Region III, the number of hits of the matrix cracking and the fibre-matrix debonding increases progressively until the global failure of the specimen. This increase is accompanied by a quasi-stabilisation of the number of hits derived from the delamination mechanism, in agreement with the steady state observed on the R-curve (Figure 5) and confirms that the GFRE composite exhibits an easier path for crack propagation due to the regular structure and the smooth surface of glass fibres (Figure 8c).

3.2.2 SEM observations

Figure 8 shows SEM images of the composite cross sections after DCB tests recorded using a Jeol JSM-IT100 SEM; several damage mechanisms identified by the AE analysis are visible. The images of the FFRE composite, which exhibits rough fibre surfaces, show the three damage mechanisms: fibre-matrix debonding, fibre and bundle failure and matrix cracking (Figures 8a and b). The images of the GFRE (Figure 8c and d) confirm the results presented in previous sections, particularly a regular structure with smooth glass fibres that explains the absence of fibre bridging, a clean delaminated surface and an easier path of crack propagation during the DCB test. Regarding the HFRE composite, a lot of torn out fibres were observed, confirming the existence of a large amount of fibre bridging (Figure 8e) requiring more energy for the propagation of cracks. In addition, Figure 8f shows some single flax fibres stretched from the flax yarns, resulting in several fibre failures, that explains the maximum value of the interlaminar toughness, G_{IC}, of the HFRE composite (Figure 5).

4. Conclusions

In this work, the mode-I interlaminar fracture toughness (G_{Ic}) of flax, glass and hybrid flax-glass fibre woven composites (FFRE, GFRE and HFRE) was studied using a DCB test and discussed. The failure mechanisms are identified using AE measurements and observed by SEM images. For the FFRE composites, the large amount of flax fibre bridging occurring during crack propagation allows an initial fracture toughness of 1.2 times more than the GFRE composite and higher delamination resistance, even though the flax fibre volume content (40%) is lower than that of glass fibres (50%). The differences in the morphology of the fibres and regularity of the structure explain these results.

The hybridisation of flax fibres with glass fibres in the composites, allows obtaining better interlaminar fracture toughness, G_{IC}, during crack propagation despite an initial value of G_{IC} close to that of GFRE and lower than the FFRE one. Thus, in HFRE laminates, glass fibres govern the initial toughness, and, then, at higher load, flax fibres play a larger role. The combination of the two types of fibres leads to deviations of the crack path, which are not observed for the other composites, probably at the origin of a greater resistance. It was also found that the initiation G_{Ic} values of the GFRE and HFRE composites were rather close despite the difference of the fibre volume content between both composites (40% for HFRE vs. 50% for GFRE). At the propagation state, the HFRE composite exhibited the largest value of G_{Ic} compared to other composites, for crack lengths between 55–85 mm. For the HFRE specimen, a large amount of fibre bridging occurred during crack propagation with a deviation in the path of the crack. However, the crack showed a clear and easy path along the fibre layer for the FFRE end GFRE composites.

The composites containing flax fibres, i.e FFRE and HFRE, display four failure mechanisms during DCB tests, whereas only three are seen for composites with glass fibres. So, the acoustic events related to glass fibres failure do not exist. Only for the hybrid composite HFRE, flax fibres are stretched due to the arrangement between flax and glass fibres, which is in agreement with the maximum value of the interlaminar toughness during the crack propagation.

In conclusion, the hybridization of glass fibres with flax fibres in a suitable combination would offer an interesting solution when toughness must be increased. In addition, reducing the weight of the

composite structure since the density of flax fibres is significantly lower than that of glass is a great advantage.

In future investigations, it would also be interesting to study the mode-II fracture toughness properties of studied composites for the purposes of finalizing this study. After that, since natural fibres are moisture sensitive, investigating the effect of wet ageing on mode-I and mode-II delamination resistance would be of interest. Another study may be interesting: analysis of the effects of through-thickness stitching on the mode-I interlaminar fracture toughness of flax and hybrid flax-glass fibre composites. In fact, the stitching process is characterised by the insertion of a through-thickness tufting yarn into the 2D perform of flax and glass fabrics. This could improve the delamination resistance in these composite materials.

Acknowledgements

The authors would like to gratefully acknowledge Cyril Marsiquet from "*Laboratoire de Physique et Mécanique Textiles"* for his technical support and contribution to the use of the SEM facility.

References

[1] L. Yan, B. Wang, B. Kasal, Can Plant-Based Natural Flax Replace Basalt and E-Glass for Fiber-Reinforced Polymer Tubular Energy Absorbers? A Comparative Study on Quasi-Static Axial Crushing, Front. Mater. 4 (2017) 1–10. doi:10.3389/fmats.2017.00042.

[2] L. Yan, N. Chouw, Crashworthiness characteristics of flax fibre reinforced epoxy tubes for energy absorption application, Mater. Des. 51 (2013) 629–640. doi:10.1016/J.MATDES.2013.04.014.

[3] L. Huang, B. Yan, L. Yan, Q. Xu, H. Tan, B. Kasal, Reinforced concrete beams strengthened with externally bonded natural flax FRP plates, Compos. Part B Eng. 91 (2016) 569–578. doi:10.1016/J.COMPOSITESB.2016.02.014.

[4] M. Ramesh, K. Palanikumar, K.H. Reddy, Plant fibre based bio-composites: Sustainable and renewable green materials, Renew. Sustain. Energy Rev. 79 (2017) 558–584. doi:10.1016/j.rser.2017.05.094.

[5] L. Yan, N. Chouw, K. Jayaraman, Effect of triggering and polyurethane foam-filler on axial crushing of natural flax/epoxy composite tubes, Mater. Des. 56 (2014) 528–541. doi:10.1016/J.MATDES.2013.11.068.

[6] L. Yan, N. Chouw, Experimental study of flax FRP tube encased coir fibre reinforced concrete composite column, Constr. Build. Mater. 40 (2013) 1118–1127. doi:10.1016/J.CONBUILDMAT.2012.11.116.

[7] L. Yan, N. Chouwa, K. Jayaraman, Flax fibre and its composites - A review Composites : Part B, Compos. Part B. 56 (2014) 296–317. doi:10.1016/j.compositesb.2013.08.014.

[8] A.K. Mohanty, M. Misra, G. Hinrichsen, Biofibres, biodegradable polymers and biocomposites: An overview, Macromol. Mater. Eng. 276–277 (2000) 1–24. doi:10.1002/(SICI)1439-2054(20000301)276:1<1::AID-MAME1>3.0.CO;2-W.

[9] K.L. Pickering, M.G.A. Efendy, T.M. Le, A review of recent developments in natural fibre composites and their mechanical performance, Compos. Part A Appl. Sci. Manuf. 83 (2016) 98–112. doi:10.1016/J.COMPOSITESA.2015.08.038.

[10] A. Le Duigou, P. Davies, C. Baley, Replacement of Glass / Unsaturated Polyester Composites By Flax / PLLA Biocomposites : Is It Justified ?, J. Biobased Mater. Bioenergy. 5 (2011) 1–17. doi:10.1166/jbmb.2011.1178.

[11] A. Lefeuvre, A. Bourmaud, L. Lebrun, C. Morvan, C. Baley, A study of the yearly reproducibility of flax fiber tensile properties, Ind. Crops Prod. 50 (2013) 400–407. doi:10.1016/j.indcrop.2013.07.035.

[12] K. Cheour, M. Assarar, D. Scida, R. Ayad, X.L. Gong, Effect of water ageing on the mechanical and damping properties of flax-fibre reinforced composite materials, Compos. Struct. 152 (2016) 259–266. doi:10.1016/j.compstruct.2016.05.045.

[13] M.R. Sanjay, P. Madhu, M. Jawaid, P. Senthamaraikannan, S. Senthil, S. Pradeep, Characterization and Properties of Natural Fiber Polymer Composites: A Comprehensive Review, J. Clean. Prod. 172 (2017) 566–581. doi:10.1016/j.jclepro.2017.10.101.

[14] T. Väisänen, O. Das, L. Tomppo, A review on new bio-based constituents for natural fiber-polymer composites, J. Clean. Prod. 149 (2017) 582–596. doi:10.1016/j.jclepro.2017.02.132.

[15] M. Fortea-Verdejo, E. Bumbaris, C. Burgstaller, A. Bismarck, K.Y. Lee, Plant fibre-reinforced polymers: where do we stand in terms of tensile properties?, Int. Mater. Rev. 62 (2017) 441–464. doi:10.1080/09506608.2016.1271089.

[16] Y. Li, X. Yi, T. Yu, G. Xian, An overview of structural-functional-integrated composites based on the hierarchical microstructures of plant fibers, Adv. Compos. Hybrid Mater. (2018) 1–16. doi:10.1007/s42114-017-0020-3.

[17] J. Merotte, A. Le Duigou, A. Kervoelen, A. Bourmaud, K. Behlouli, O. Sire, C. Baley, Flax and hemp nonwoven composites: The contribution of interfacial bonding to improving tensile properties, Polym. Test. 66 (2018) 303–311. doi:10.1016/j.polymertesting.2018.01.019.

[18] C. Fragassa, F.V. de Camargo, A. Pavlovic, G. Minak, Experimental evaluation of static and dynamic properties of low styrene emission vinylester laminates reinforced by natural fibres, Polym. Test. 69 (2018) 437–449. doi:10.1016/j.polymertesting.2018.05.050.

[19] F. Bensadoun, I. Verpoest, A.W. Van Vuure, Interlaminar fracture toughness of flax-epoxy

composites, J. Reinf. Plast. Compos. 36 (2017) 121–136. doi:10.1177/0731684416672925.
[20] M. Pinto, V.B. Chalivendra, Y.K. Kim, A.F. Lewis, Improving the strength and service life of jute/epoxy laminar composites for structural applications, Compos. Struct. 156 (2016) 333–337. doi:10.1016/j.compstruct.2015.10.005.
[21] M. Ravandi, W.S. Teo, L.Q.N. Tran, M.S. Yong, T.E. Tay, The effects of through-the-thickness stitching on the Mode I interlaminar fracture toughness of flax/epoxy composite laminates, Mater. Des. 109 (2016) 659–669. doi:10.1016/j.matdes.2016.07.093.
[22] Y. Zhang, Y. Li, H. Ma, T. Yu, Tensile and interfacial properties of unidirectional flax / glass fiber reinforced hybrid composites, Compos. Sci. Technol. 88 (2013) 172–177.
[23] Z. Khan, B.F. Yousif, M. Islam, Fracture behaviour of bamboo fiber reinforced epoxy composites, Compos. Part B Eng. 116 (2017) 186–199. doi:10.1016/J.COMPOSITESB.2017.02.015.
[24] F.A. Almansour, H.N. Dhakal, Z.Y. Zhang, Effect of water absorption on Mode I interlaminar fracture toughness of flax/basalt reinforced vinyl ester hybrid composites, Compos. Struct. 168 (2017) 813–825. doi:10.1016/j.compstruct.2017.02.081.
[25] F.A. Almansour, H.N. Dhakal, Z.Y. Zhang, Investigation into Mode II interlaminar fracture toughness characteristics of flax/basalt reinforced vinyl ester hybrid composites, Compos. Sci. Technol. 154 (2018) 117–127. doi:10.1016/j.compscitech.2017.11.016.
[26] C. Chen, Y. Li, T. Yu, Interlaminar toughening in flax fiber-reinforced composites interleaved with carbon nanotube buckypaper, J. Reinf. Plast. Compos. 33 (2014) 1859–1868. doi:10.1177/0731684414548084.
[27] A. Le Duigou, P. Davies, C. Baley, Macroscopic analysis of interfacial properties of flax/PLLA biocomposites, Compos. Sci. Technol. 70 (2010) 1612–1620. doi:10.1016/j.compscitech.2010.06.001.
[28] E.H. Saidane, D. Scida, M. Assarar, R. Ayad, Damage mechanisms assessment of hybrid flax-glass fibre composites using acoustic emission, Compos. Struct. 174 (2017) 1–11. doi:10.1016/j.compstruct.2017.04.044.
[29] A. Monti, A. El Mahi, Z. Jendli, L. Guillaumat, Mechanical behaviour and damage mechanisms analysis of a flax-fibre reinforced composite by acoustic emission, Compos. Part A Appl. Sci. Manuf. 90 (2016) 100–110. doi:10.1016/J.COMPOSITESA.2016.07.002.
[30] M. Assarar, D. Scida, W. Zouari, E.H. Saidane, R. Ayad, Acoustic emission characterization of damage in short hemp-fiber-reinforced polypropylene composites, Polym. Compos. 37 (2016) 1101–1112. doi:10.1002/pc.23272.
[31] M. Haggui, A. El Mahi, Z. Jendli, A. Akrout, M. Haddar, Static and fatigue characterization of flax fiber reinforced thermoplastic composites by acoustic emission, Appl. Acoust. (2018). doi:10.1016/J.APACOUST.2018.03.011.
[32] ASTM D5528-13, Standard Test Method for Mode I Interlaminar Fracture Toughness of Unidirectional Fiber-Reinforced Polymer Matrix Composites, ASTM International, West Conshohocken, PA, 2013, www.astm.org. doi: 10.1520/D5528-13.
[33] A. Bravo, L. Toubal, D. Koffi, F. Erchiqui, Characterization of Tensile Damage for a Short Birch Fiber-reinforced Polyethylene Composite with Acoustic Emission, Int. J. Mater. Sci. 3 (2013) 79–89.
[34] A. Bravo, L. Toubal, D. Koffi, F. Erchiqui, Development of novel green and biocomposite materials: Tensile and flexural properties and damage analysis using acoustic emission, Mater. Des. 66 (2015) 16–28. doi:10.1016/J.MATDES.2014.10.026.
[35] M. Habibi, G. Lebrun, L. Laperrière, Experimental characterization of short flax fiber mat composites: tensile and flexural properties and damage analysis using acoustic emission, J. Mater. Sci. 52 (2017) 6567–6580. doi:10.1007/s10853-017-0892-1.
[36] F. Meraghni, M.L. Benzeggagh, Micromechanical modelling of matrix degradation in randomly oriented discontinuous-fibre composites, Compos. Sci. Technol. 55 (1995) 171–186. doi:10.1016/0266-3538(95)00096-8.
[37] M.R. Mitchell, R.E. Link, V. Arumugam, C.S. Kumar, C. Santulli, F. Sarasini, A.J. Stanley, A Global Method for the Identification of Failure Modes in Fiber glass Using Acoustic Emission, J. Test. Eval. 39 (2011) 103730. doi:10.1520/JTE103730.

Figures

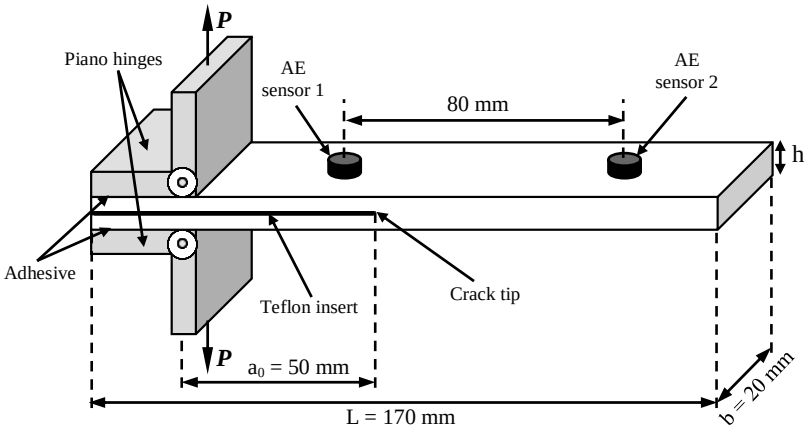

(a)

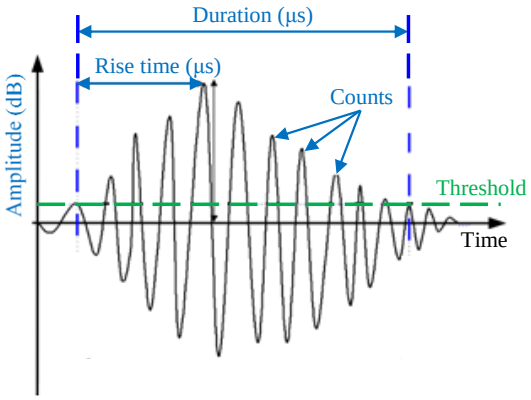

(b)

Figure 1. a) Geometry and nominal dimensions of specimen for mode-I DCB test, b) AE waveform

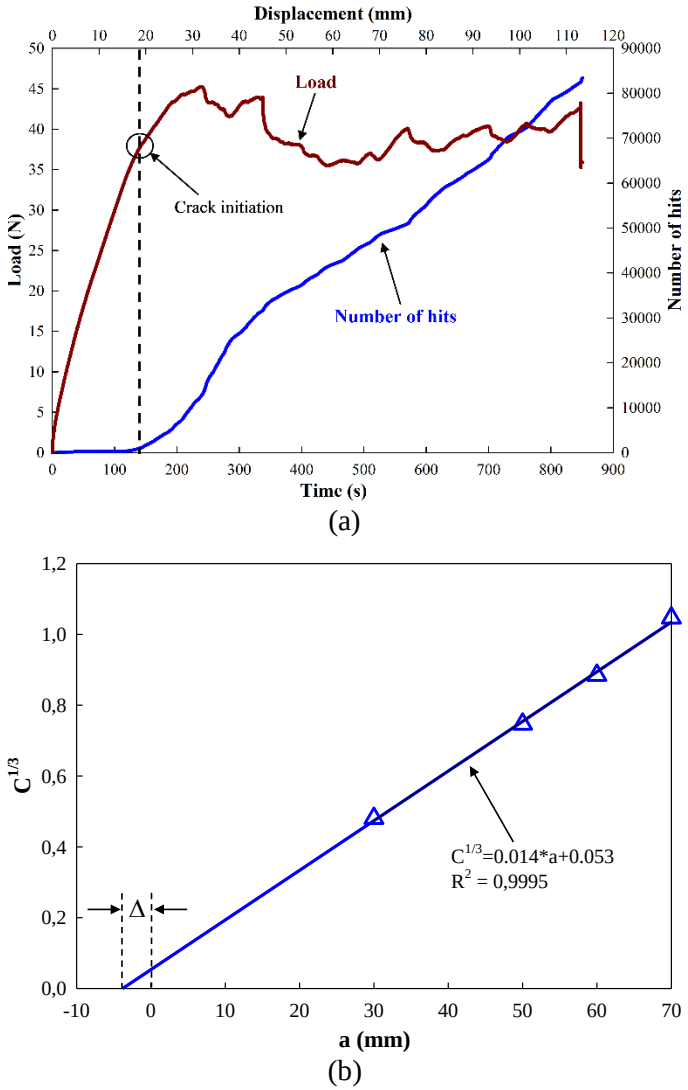

Figure 2. Mode-I DCB calibration for FFRE: a) Crack propagation onset, b) MBT

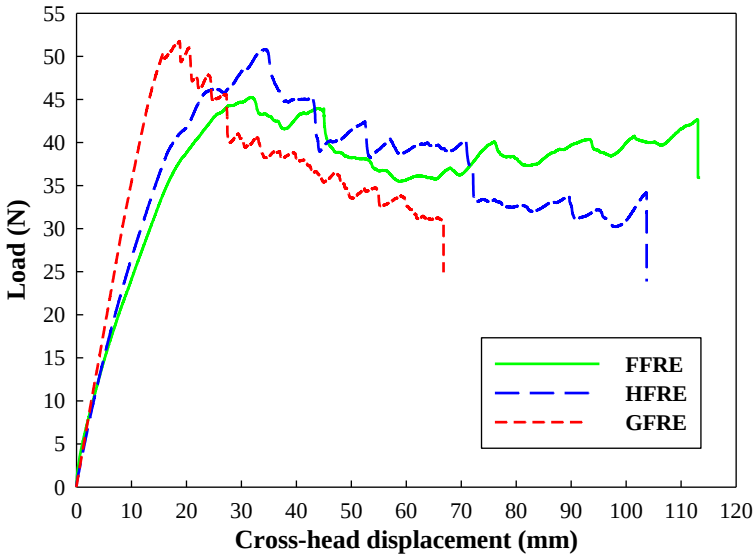

Figure 3. Experimental load-displacement response for the FFRE, HFRE and GFRE composites

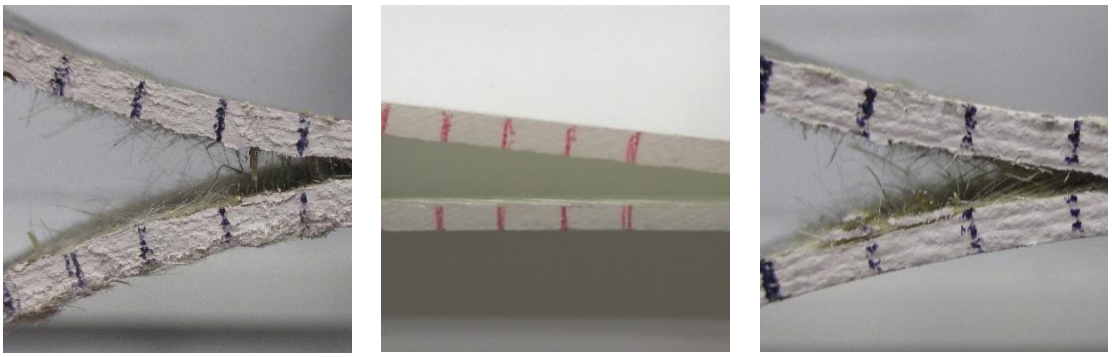

(a) (b) (c)

Figure 4. Typical pictures of composites at midplane interface of the DCB test: a) FFRE, b) GFRE, c) HFRE specimens

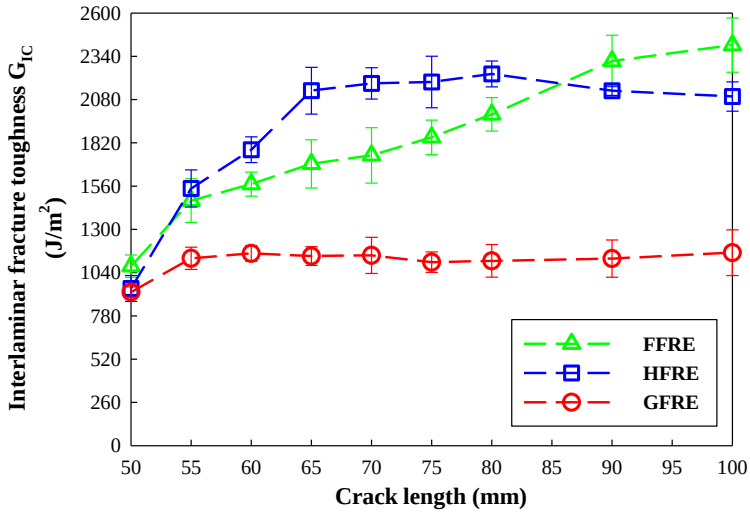

Figure 5. R-curve from the DCB test for the FFRE, HFRE and GFRE specimens

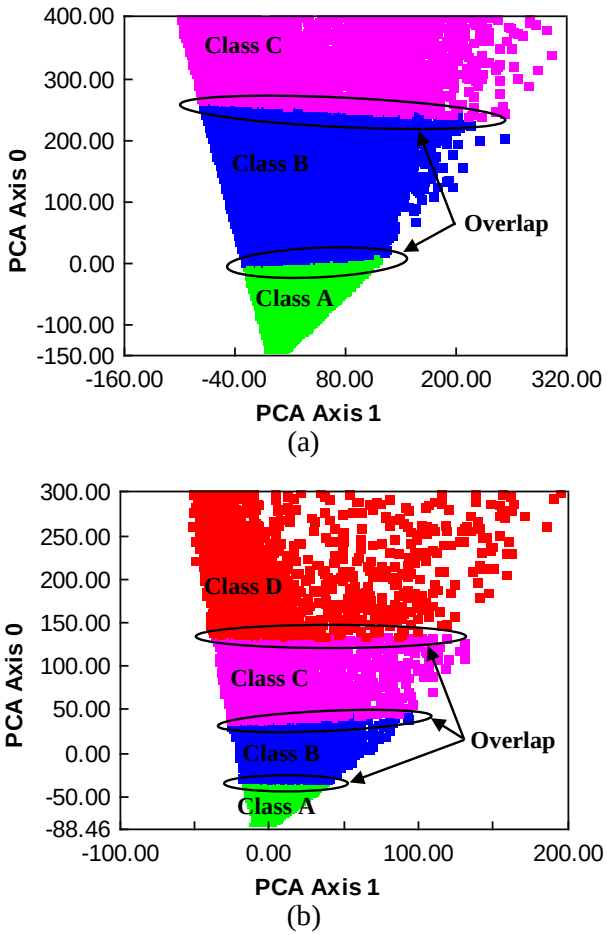

Figure 6. Principal component analysis (PCA) visualisation of the AE clustering of the mode-I DCB test for: a) GFRE, b) FFRE specimens

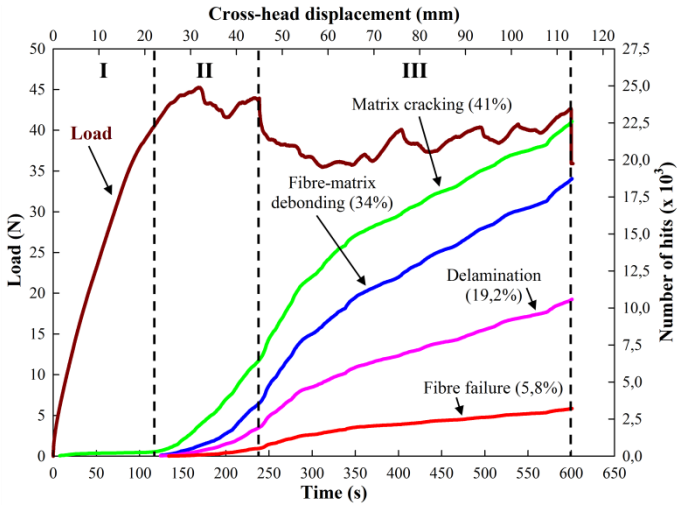

(a)

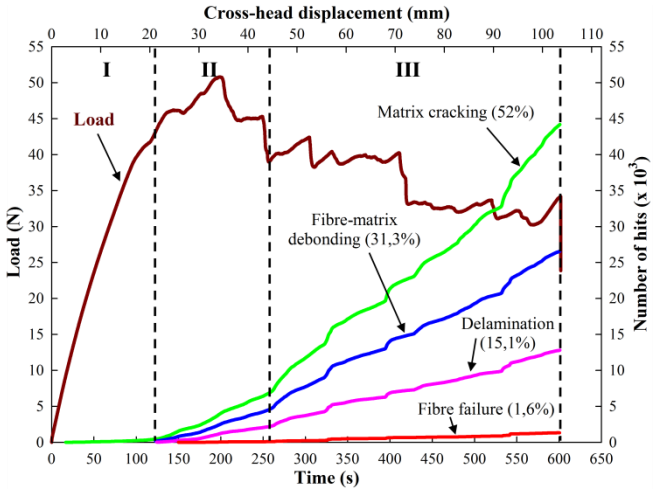

(b)

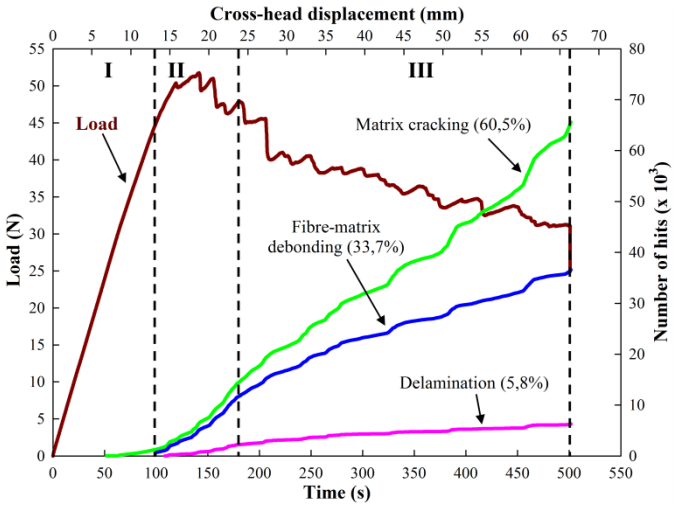

(c)

Figure 7. Load and cumulative number of hits of the AE signals versus time and cross-head displacement from DCB tests for: a) FFRE, b) HFRE, c) GFRE specimens

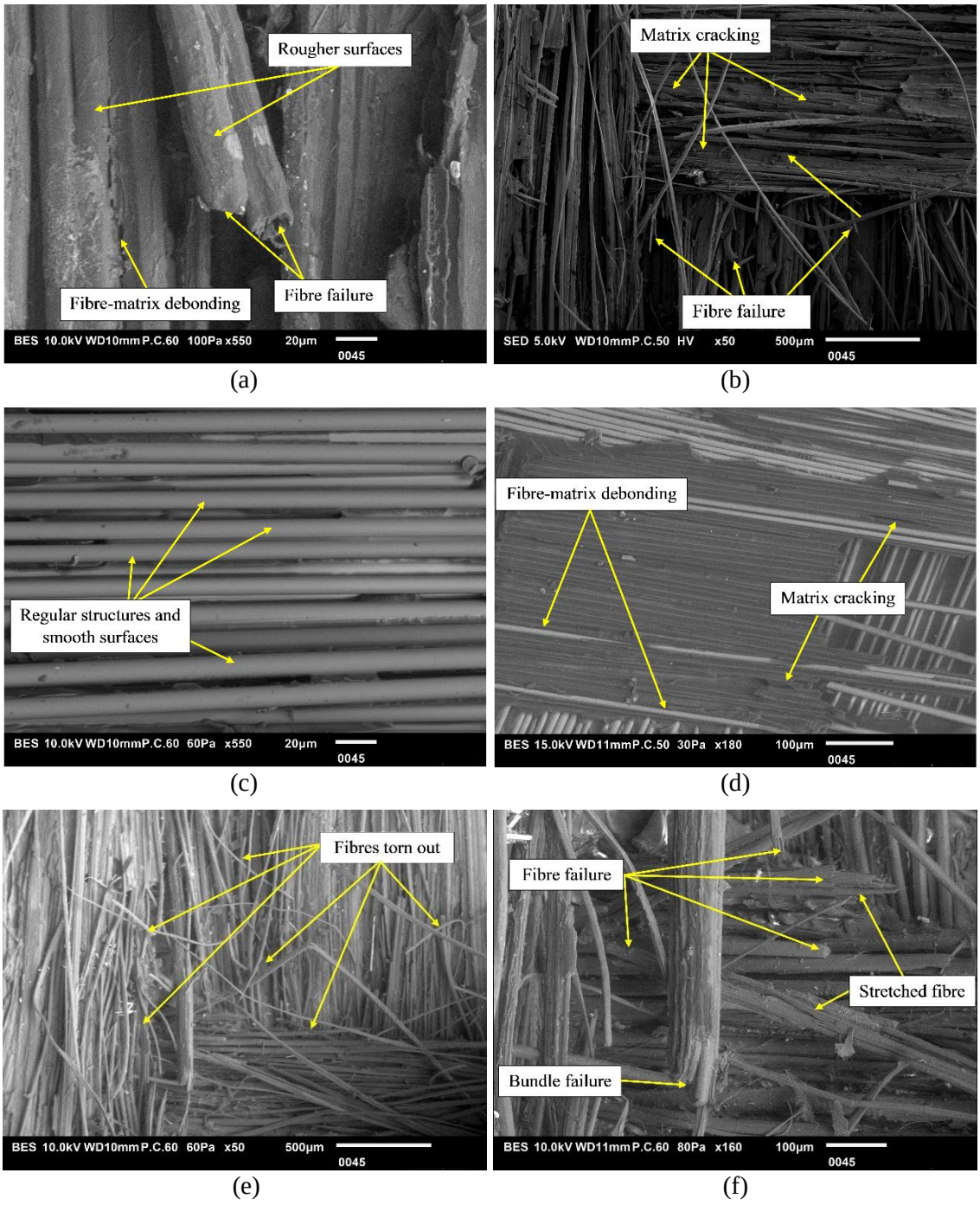

Figure 8. SEM pictures taken from the fracture surfaces: a and b) FFRE, c and d) GFRE, e and f) HFRE specimens

Tables

Table 1. Layer configuration, nominal thickness and fibre volume content of studied laminates

Laminate designation	Number of plies (flax/glass)	Layer configuration	Nominal thickness (mm) (flax/glass)	Fibre volume content V_f (flax/glass)
FFRE	10/0	$[F_5]_s$	4.98/0.00	0.40/0.00
HFRE	6/6	$[(G/F)_6]$	3.21/1.35	0.26/0.14
GFRE	0/20	$[G_{10}]_s$	0.00/4.17	0.00/0.50

F: Flax fabric, G: Glass fabric, s: symmetric stacking sequences.

Table 2. Density, values of initiation fracture toughness and specific fracture toughness (the ratio of G_{Ic} to the material density) for the studied laminates

Material	Density of composite (kg/m^3)	Fracture toughness (J/m^2)	Specific fracture toughness ($x\ 10^{-3}$ J.m/kg)
FFRE	1272.1 ± 8.1	1079.2 ± 66.4	848.40 ± 5.34
HFRE	1411.5 ± 13.1	944.8 ± 76.7	669.40 ± 6.17
GFRE	1888.4 ± 10.4	922.9 ± 30.2	488.70 ± 2.68

Table 3. AE characteristics of each signal clustering for all composites

Material	AE parameter	Class A	Class B	Class C	Class D
FFRE	Amplitude (dB)	32–50	40–65	50–78	75–92
	Duration (μs)	5–59	48–123	115–221	204–600
	Counts	1–34	26–98	36–110	29–171
	Energy (aJ)	1–70	60–900	1000–9000	>100000
HFRE	Amplitude (dB)	32–55	39–66	52–82	78–99
	Duration (μs)	8–62	60–216	211–331	204–620
	Counts	1–38	24–104	38–113	39–182
	Energy (aJ)	1–80	60–1000	900–10000	>100000
GFRE	Amplitude (dB)	32–60	42–68	55–80	
	Duration (μs)	10–70	52–200	142–300	
	Counts	1–30	18–107	41–169	
	Energy (aJ)	1–100	60–1200	1400–12000	